J. Indian Inst. Sci., Mar.–Apr. 1997, **77**, 181–189.

Steady flow past a circular cylinder with parabolic velocity distribution at high reynolds numbers — A numerical study

C. V. RAGHAVARAO
Department of Mathematics, Indian Institute of technology, Madras, 600 036, India
AND
Y. V. S. S. SANYASIRAJU
Department of Mathematics, Indian Institute of technology, Guwahati, 781 001, India.

Abstract

A steady, viscous, incompressible flow past a circular cylinder is studied numerically at moderately high Reynolds numbers. A variable shear flow with velocity curvature factor G is taken as the incident flow. The drag coefficient is calculated at Re = 1000 and 2000 with G = 0, 0.1 and 1.0. The results for G = 0, which correspond to uniform flow, are compared with the existing results for Reynolds numbers upto 500. The non-zero curvature is found to affect the breadth of the wake bubble, the separation angle and the drag coefficient.

Keywords: Parabolic velocity distribution, Steady flow, viscous, shear, Finite difference method, Block SLOR method.,

1. Introduction

Steady, viscous, incompressible flow past a circular cylinder is one of the classical problems in fluid dynamics. Many authors have studied the unsteady flow past a circular cylinder. The existing unsteady flow investigations show that at moderate and high Reynolds numbers the flow does not tend to a steady state even after a long time. Very little work has been reported for the steady state problem at high Reynolds numbers. This has motivated the authors to consider this particular problem. Fornberg[4] considered the steady flow past a stationary circular cylinder, and has given the flow patterns and drag coefficient values up to Reynolds number 600. Tang and Ingham considered the steady flow past a rotating circular cylinder up to Reynolds number 100. Steady solutions have been obtained by Fornberg[5] (1988) for the flow past a sphere at Reynolds numbers as high as 5000.

The complete literature survey on this problem was given by Collins *et al.*[2] and Fornberg[4]. Collins and Dennis[2], Badr and Dennis[1], Loc *et al*[7,8]. and Son *et al*[9]. are some of the investigators who have studied numerically the unsteady flow past an impulsively started circular cylinder.

In the present investigation we study the effect of shear in the incident flow. We consider a parabolic velocity profile characterized by a velocity curvature factor G. For G = 0 the incident flow is uniform, and the present results can be compared with those of Fornberg[4] and Tang *et al.*

The basic parameters entering into the variable shear flow are the Reynolds number defined as $\mathrm{Re} = \frac{2Ua}{\nu}$ where ν is the coefficient of kinematic viscosity, U is the characteristic velocity of the fluid, and a is the characteristic length (radius of the cylinder in the present case) and the velocity curvature factor G. Streamlines, vorticity contours and drag coefficient values are presented. The drag coefficients obtained are compared with those from 24 Fornberg[4] and Tang *et al.* for Reynolds numbers ranging from 20 to 500.

Formulation of the problem

For steady, viscous, incompressible flow past a circular cylinder, the flow at sufficiently large distances with variable shear is shown in Figure 1. The problem is described in cartesian and polar co-ordinate systems with the origin on the axis of the cylinder. It is a two-dimensional flow such that the flow in the planes z = constant are the same. The velocity components at sufficiently large distances are,

$$u' = \frac{\partial \psi'(x', y')}{\partial y'} = U\left(1 + G\frac{y'^2}{a^2}\right),$$

$$v' = -\frac{\partial \psi'(x', y')}{\partial x'} = 0, \tag{1}$$

where ψ' is a stream function, a, the characteristic length (radius of the cylinder), U, the characteristic velocity of the fluid, and G, the velocity curvature factor; primes denote dimensional quantities. All quantities in the r-θ plane are non-dimensionalized as

$$r = \frac{r'}{a}, u = \frac{u'}{U}, \psi = \frac{\psi'(r, \theta)}{aU}$$

giving Re = 2 Ua/ν.

The dimensionless governing differential equations for the two-dimensional flow in the stream function-vorticity formulation in the r-θ plane are

$$\nabla^2 \psi = -\omega$$

$$\nabla^2 \omega = -\frac{\mathrm{Re}}{2r}\frac{\partial(\psi, \omega)}{\partial(r.\theta)}, \tag{2}$$

where

$$\nabla^2 = \frac{\partial^2}{\partial r^2} + \frac{1}{r}\frac{\partial}{\partial \pi} + \frac{1}{r^2}\frac{\partial^2}{\partial \theta^2},$$

$$v_r = \frac{1}{r}\frac{\partial \psi}{\partial \theta}, v_e = -\frac{\partial \psi}{\partial r}.$$

The boundary conditions are

$\psi = \frac{\partial \psi}{\partial r} = 0$ on the surface of the cylinder

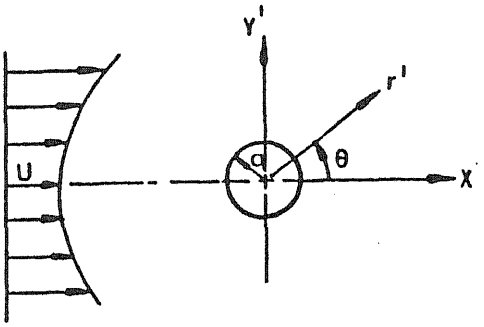

FIG. 1. Schematic of cylinder in flow field.

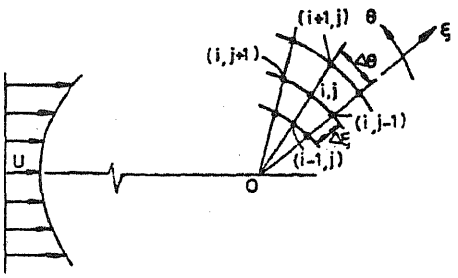

FIG. 2. Finite different mesh.

$$\psi = r\sin\theta + G\frac{r^3}{3}\sin^3\theta \text{ as } r \to \infty$$

$$\omega = -2G\sin\theta \qquad \text{as } r \to \infty$$

For G = 0 the boundary conditions represent uniform flow past a circular cylinder. The condition for vorticity ω on the surface of the cylinder is deduced using the definition of ω and the zero velocity on the surface, i.e. $\dfrac{\partial\psi}{\partial r} = 0$.

Numerical approximation

The governing coupled differential equations are solved numerically using an upwind finite difference scheme. The stream function ψ and vorticity ω vary rapidly near the cylinder surface and hence a smaller step size is essential in this region of the flow field. Far away from this surface larger step sizes are permissible. To meet this requirement, the independent variables r and θ are transformed as

$$r = e^{\pi\xi} \text{ and } \theta = \pi\eta.$$

With these transformations the governing differential equations (3) take the form

$$\nabla^2\psi = -\pi^2 e^{2\pi\xi}\omega$$

$$\nabla^2\omega = -\frac{\mathrm{Re}}{2}\frac{\partial(\psi,\omega)}{\partial(\xi,\eta)}, \tag{4}$$

where

$$\nabla^2 = \frac{\partial^2}{\partial\xi^2} + \frac{\partial^2}{\partial\eta^2},$$

$$v_r = e^{-\pi\xi}\frac{\partial\psi}{\partial\eta}, v_\theta = -e^{-\pi\xi}\frac{\partial\psi}{\partial\xi}.$$

The boundary conditions now read

$$\psi = \frac{\partial\psi}{\partial\xi} = 0 \text{ on the surface of the cylinder}$$

$$\psi = e^{\pi\xi}\sin\pi\eta + \frac{G}{3}e^{3\pi\xi}\sin^3\pi\eta \text{ as } \xi \to \xi_\infty,$$

$$\omega = -2G\sin\pi\eta \qquad \text{as } \xi \to \xi_\infty$$

where ξ_∞ is the artificial outer boundary. The condition on the surface of the cylinder for vorticity comes from $\frac{\partial\psi}{\partial\xi} = 0$.

The finite difference discretization of the ξ–η domain is given in figure 2. The nodal points are the points of intersection of ξ = constant (circles) and η = constant (lines). The second order derivatives are approximated by central differences of order $\Delta\xi^2$ or $\Delta\eta^2$, where $\Delta\xi$ and $\Delta\eta$ are the step lengths in ξ and η directions respectively. The nonlinear terms in the coupled equations are approximated with first-order upwind differences of the form,

$$(fF)_\xi = .5(f - |f|)F_{i+1,j} + |f|F_{i,j} - .5(f + |f|)F_{i-1,j} \tag{5}$$

where f stands for the coefficients of the first-order partial derivatives of ω. These coefficients are derivatives of ψ that have been approximated with central differences at any point (ξ_i, η_j). F is the vorticity ω. The boundary condition on the surface of the cylinder is taken as

$$\omega_{0,j} = -\frac{8\psi_{1,j} - \psi_{2,j}}{2\pi^2(\Delta\xi)^2} \tag{6}$$

where j is the node number in η direction and 0, 1 and 2 are the nodes in ξ direction.

The Block SLOR method is used in the iteration process. The resulting algebraic equations obtained for ω and ψ are solved in the same order using a tridiagonal solver along each line. Diagonal dominance is assured because of the upwind difference approximation for the non-linear terms, even at high Reynolds numbers. These iterations are continued until,

$$\left|F^{(n+1)} - F^{(n)}\right| \le 10^{-4} \tag{7}$$

at all inner grid points for all field variables ψ and ω. Here n is the iteration number.

To minimize the oscillations of the solution in the convergence process it is necessary to use some initial solution in the iteration process. Here, we used the inviscid flow solution to solve the coupled equations at small Reynolds numbers, say at Re = 10, and this solution was used as the starting solution at high Reynolds numbers. The optimum acceleration parameters in the convergence process were found to be .8 and .6 for stream function ψ and vorticity ω, respectively. In order to assess the validity of the grid, grid independence tests have been conducted with 41×81, 61×121 and 81×161 grids. For a typical case of Re = 60 and G = 0, the maximum vorticity has been compared between these grids. These values are obtained as 7.094, 7.33 and 7.44, respectively for the three grids. Because of the 3% variation of the maximum vorticity between the first two grids,

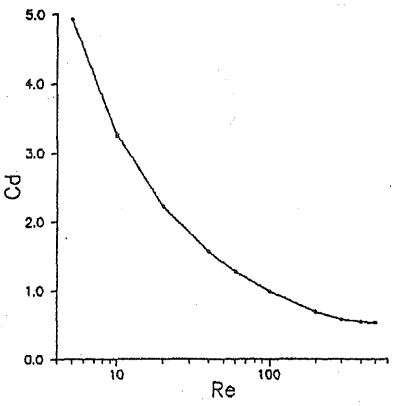

FIG. 3. Drag coefficient as a function of Re.

Table 1
Comparison of drag coefficient at moderate Reynolds numbers

Re	Present results C_D	Ref. 6, 10 C_D	Ref. 4 C_D
20	2.229	1.995	—
60	1.279	1.279	—
100	0.986	1.059	1.060
500	0.529	—	0.528

an 81 × 161 grid is used for all calculations. With 3 this grid at Re = 10 the present code requires 15 minutes of CPU time on an HP9000 workstation.

Discussion of the results

With $\xi_\infty = 0.81$ and G = 0, the code was tested at 98 moderate Reynolds numbers ($20 \le Re \le 500$) by comparing the resulting flow patterns with the results of Ingham *et al*[6]. and Tang *et al*[10]. For Reynolds numbers 60 and 100 the location of separation on the surface of the cylinder was obtained as 63° and 70°, respectively. The variation of the drag with Reynolds number is given in figure 3 and tabulated in Table 1 along with the values of Ingham *et al.*[6], Tang *et al*[10]. and Fornberg. We observed that agreement is satisfactory.

The results for Re = 1000 and 2000 with G = 0, 0.1 and 1.0 have been obtained. The corresponding streamlines and vorticity contours are presented in figures 4 to 7 for different values of Reynolds numbers and curvature factor G. In figures 4 and 5 the streamlines and vorticity contours at Re = 1000 are given close to the cylindrical surface to show the flow pattern clearly. To give an overall picture of the flow pattern the graphs at Re = 2000 are given in a wider range −10 to 10 in x direction and −4 to 4 in y direction. For uniform flow, *i.e.*, for G = 0, it is found from these results that the length and breadth of the wake bubble increases with the Reynolds number. The separation of the flow occurs at 91° and 95.8° for Re = 1000 and 2000, respectively. The symmetry of the flow is observed even at high Reynolds numbers. The same is also observed for the variable shear flow with velocity curvature factor G = 0.1 and 1.0. To confirm the validity of the present results these results are compared with the results obtained by approximating the convective terms with second order upwind difference method of the form

$$(fF)_\xi = \frac{(f+|f|)}{2}\left(\frac{-3F_{i,j}+F_{i+1,j}-F_{i+2,j}}{2\Delta\xi}\right)+\frac{(f-|f|)}{2}\left(\frac{3F_{i,j}-4F_{i-1,j}+F_{i-2,j}}{2\Delta\xi}\right) \qquad (8)$$

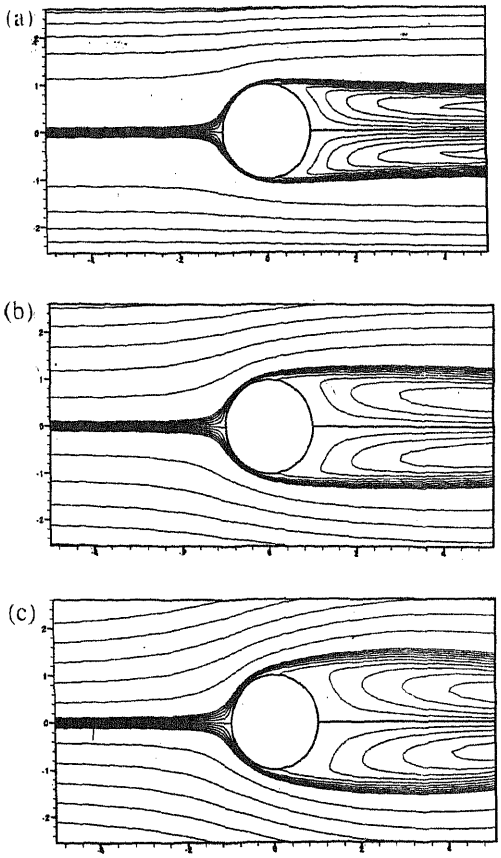

FIG. 4. Streamlines as Re = 1000, (a) G = 0.0, ψ = (−2 to 2), (b) G = 0.1, ψ = (−3 to 3), (c) G = 1.0, ψ = (−8 to 8).

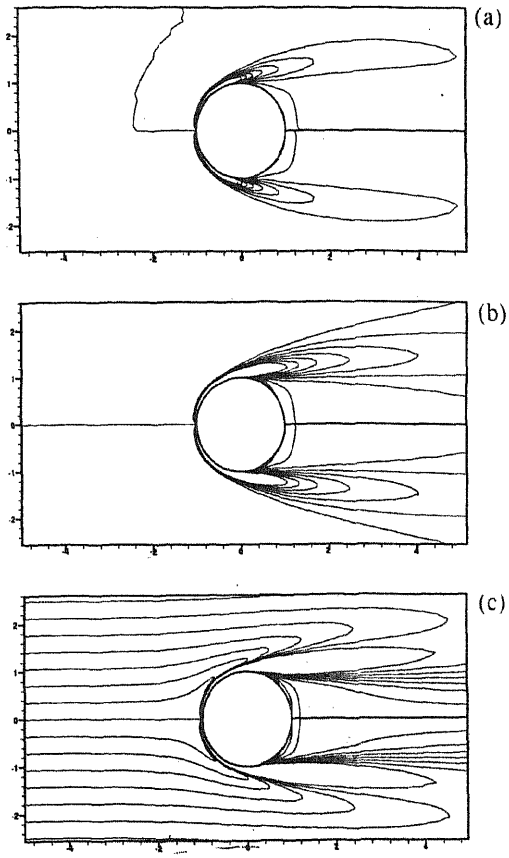

FIG. 5. Vorticitycontours at Re = 1000, (a) G = 0.0, ω = (−7 to 7), (b) G = 0.1, ω = (−4 to 4), (c) G = 1.0, ω = (−5 to 5).

where f and F are defined earlier in equation (5). With this approximation it is observed that the results obtained up to Re = 2000 do not vary much but at higher values they varied considerably.

The streamlines at Re = 1000 and 2000 in figures 4 and 6 show the wake region reduced in length and breadth as G increases. Particularly, the breadth is decreased drastically with increasing G for all Re. But, away from the surface of cylinder the flow is almost similar to the uniform flow. The distortion in vorticity distribution due to the cylinder in shear flow is given in figures 5 and 7. Unlike uniform flow the vorticity is distrib-

Table 2
Separation angles at various Reynolds numbers

Re	G = 0	G = 0.1	G = 1.0
1000	91°	84°	74°
2000	95.8°	87°	79.3°

Table 3
Drag coefficient at various Reynolds numbers

Re	G = 0	G = 0.1	G = 1.0
1000	0.476	1.359	4.592
2000	0.284	0.754	2.581

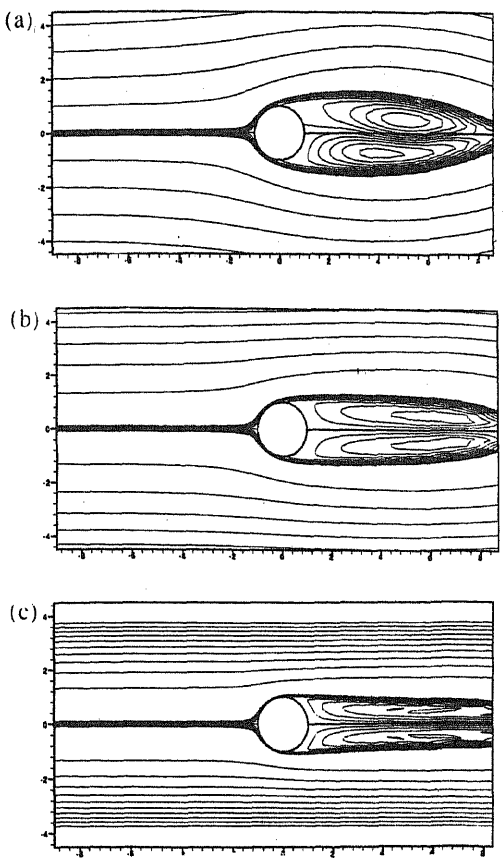

FIG. 6. Streamlines as Re = 2000, (a) G = 0.0, ψ = (−5 to 5), (b) G = 0.1, ψ = (−7 to 7), (c) G = 1.0, ψ = (−21 to 21).

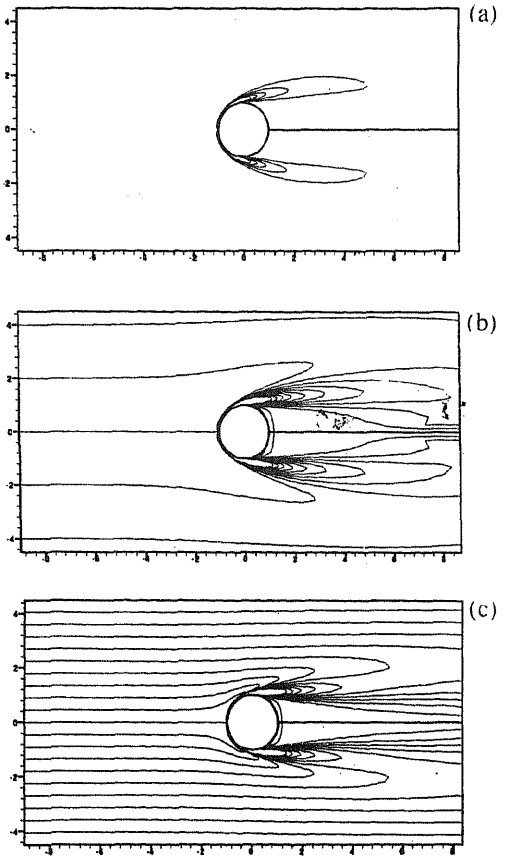

FIG. 7. Vorticitylines at Re = 2000, (a) G = 0.0, ω = (−5 to 5), (b) G = 0.1, ω = (−4 to 4), (c) G = 1.0, ω = (−9 to 9).

uted throughout the domain because of the nature of the incident flow. The vorticity contours near the surface of the cylinder are turned towards the cylinder at the top and bottom. In figure 5 the closed vorticity contours near the cylinder are given at Re = 1000 and G = 0, 0.1 and 1.0. The separation angles are reported in Table II for various G.

The drag coefficient C_D is calculated in terms of frictional drag and pressure drag of the form $C_D = C_{DF} + C_{DP}$ at $\xi = 0$ as

$$C_D = -\int_0^{2\pi} P\cos\theta \, d\theta - \frac{2}{\mathrm{Re}}\int_0^{2\pi} \omega \sin\theta \, d\theta. \tag{9}$$

where the non-dimensionalized pressure P is calculated from the relation

$$\frac{\partial P}{\partial \eta} = \frac{2}{\mathrm{Re}}\frac{\partial \omega}{\partial \xi}. \tag{10}$$

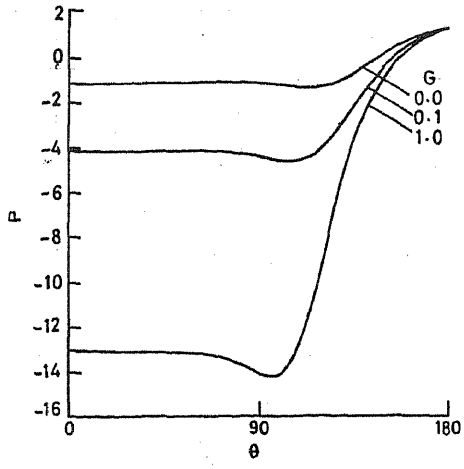

FIG. 8. Pressure coefficient on the cylinder at Re = 1000.

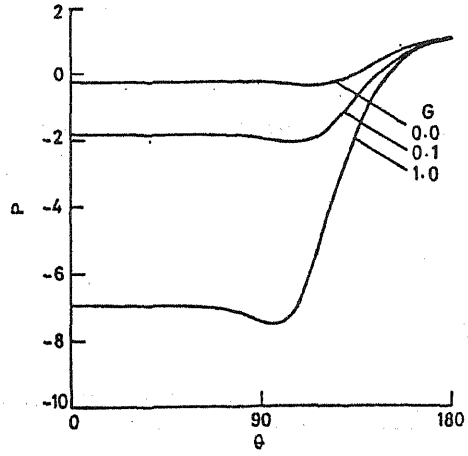

FIG. 9. Pressure coefficient on the cylinder at Re = 2000.

The integrals in (9) are evaluated by using integration by parts. Then we have

$$C_D = \frac{2}{\mathrm{Re}} \int_0^{2\pi} \frac{\partial \omega}{\partial \xi} \sin\theta \, d\theta - \frac{2}{\mathrm{Re}} \int_0^{2\pi} \omega \sin\theta \, d\theta \tag{11}$$

With these relations it is observed that the drag coefficient C is increasing with G.The resulting drag D coefficients are given in table 3.

To see the effect of G on the pressure, the dimensionless pressure coefficients defined by (White[11] (1974))

where $p_0(\theta)$ is the pressure on the cylinder surface and p_∞, the uniform pressure at large distances, is calculated from the formula

$$P(\theta) = 1 + \frac{8\pi}{\mathrm{Re}} \int_0^{\infty} \frac{\partial \omega}{\partial \xi}\bigg|_{\theta=\pi} d\xi - \frac{4}{\mathrm{Re}} \int_\theta^{\pi} \frac{\partial \omega}{\partial \xi}\bigg|_{\xi=0} d\theta \tag{13}$$

The curves of the pressure coefficient at Re = 1000 and 2000 for various G are given in figures 8 and 9, respectively.

Conclusions

Steady viscous flow past a circular cylinder with a parabolic velocity distribution is considered for high Reynolds numbers. The main observations of the present results are:

1. The breadth of the wake bubble decreases with increasing G. As a result the separation angle also decreased with increasing G - separation occurs further downstream.
2. Drag coefficient increases with G.

Acknowledgement

The authors are grateful to the referees for their comments which helped in improving the quality of the paper.

References

1. BADR, H. M. AND DENNIS, S. C. R. — Time-dependent viscous flow past an impulsively started rotating and translating circular cylinder, J. Fluid Mech., 1985, **158**, 447–488.

2. COLLINS, W. M. AND DENNIS, S. C. R. — Flow past an impulsively started cylinder, *J. Fluid Mech.*, 1973, **60**, 105–127

3. DENNIS, S. C. R. AND CHANG, G. Z. — Numerical solutions for steady flow past a circular cylinder at Reynolds number up to 100, *J. Fluid Mech.*, 1970, **42**, 471–489.

4. FORNBERG, B. — Steady viscous flow past a circular cylinder up to Reynolds numbers 600, *J. Comp. Phys.*, 1985, **61**, 297–320.

5. FORNBERG, B. — Steady viscous flow past a sphere at high Reynolds numbers, *J. Fluid Mech.* 1988, **190**, 1471–489.

6. INGHAM, D. B. AND TANG, T. — A numerical investigation into the steady flow past a rotating circular cylinder at low and intermediate Reynolds numbers, *J. Comp. Phys.*, 1990, **87**, 91–107.

7. LOC, T. P. — Numerical analysis of unsteady secondary vortices generated by an impulsively started circular cylinder, *J. Fluid Mech.*, 1980, **100**, 111–128.

8. LOC, T. P. AND BOARD, R. — Numerical solution of the early stage of the unsteady viscous flow around a circular cylinder : A comparison with experimental visualization and measurements, *J. Fluid Mech.*, 1980, **160**, 193–117.

9. SON, J. S. AND HANRATTY, T. J. — Numerical solution for the flow around a cylinder at Re of 40, 200 and 500, *J. Fluid Mech.*, 1969, **35**, 369–386.

10. TANG, T. AND INGHAM, D. B. — On steady flow past a rotating circular cylinder at Reynolds numbers 60 and 100, *Comp. Fluids*, 1991, **19**, 217–230.

11. WHITE, F. M. — *Viscous Fluid Flow*, McGraw Hill, 1974.